Available online at www.sciencedirect.com
SCIENCE DIRECT
Journal of Catalysis 238 (2006) 489–496
JOURNAL OF CATALYSIS
www.elsevier.com/locate/jcat

Low-temperature water–gas shift reaction over cobalt–molybdenum carbide catalyst

Masatoshi Nagai *, Kenji Matsuda

Graduate School of Bio-applications and Systems Engineering, Tokyo University of Agriculture and Technology, 2-24 Nakamachi, Koganei, Tokyo 184-8588, Japan

Received 5 August 2005; revised 19 December 2005; accepted 3 January 2006

Abstract

The water–gas shift (WGS) reaction over a series of cobalt-molybdenum carbide catalysts was studied at 453 K. The cobalt-molybdenum (Co_xMo_{1-x}) oxides were prepared using a mixture of aqueous solutions of cobalt nitrate and ammonium heptamolybdate and carburized by a temperature-programmed reaction with a 20% CH_4/H_2 mixture. The catalysts were characterized using X-ray diffraction, CO adsorption, temperature-programmed carburization (TPC) with a 20% CH_4/H_2 mixture, X-ray photoelectron spectroscopy, and transmission electronic microscopy. The 873 K-carburized $Co_{0.5}Mo_{0.5}$ was found to be the most active among the Co–Mo carbide catalysts; it was more active than a commercial CuZn at 5 min but less active than CuZn at 300 min. The TPC experiment determined the reduction and/or carburization of the Mo and CoMo oxides into the carbides through the oxycarbides. The TPC of the $Co_{0.5}Mo_{0.5}$ oxide showed that the first peak of H_2O at 747 K was due to the reduction and/or carburization of MoO_3 to MoO_2 and Mo oxycarbide and of $CoMoO_4$ to the Co–Mo oxycarbide, and the second peak at 893 K was due to the carburization of the Co–Mo oxycarbide to β-Mo_2C with Co metal and amorphous Co–Mo carbide. In addition, the $Co_{0.5}Mo_{0.5}$ carbide catalyst contained β-Mo_2C, Co metal, and the amorphous Co–Mo oxycarbide (the composition of $CoMoC_{6.2}O_{1.4}$), which grew into crystallites of Co_3Mo_3C after being heated in H_2. The amorphous Co–Mo oxycarbide is responsible for the WGS reaction.

Keywords: Co–Mo; Carbide; Water–gas shift; XRD; TPC

1. Introduction

The water–gas shift (WGS) reaction is being studied as a CO-removal technology for obtaining reformed fuel from hydrocarbons and methanol, in view of its application to fuel cells. Although CuO–ZnO–Al_2O_3 is currently used commercially for the WGS reaction at low temperatures [1–6], it must be improved and replaced by other novel catalysts that exhibit higher resistance to sulfur compounds in the feeds and to deactivation by oxygen and water. Other metal-based catalysts, including Fe [7], Ni [8], Li–Mg [9], Cu/Mn [10], and Mo catalysts [11–14], have been investigated to ascertain their suitability for the WGS reaction. The molybdenum-containing catalysts exhibited high performance at high temperature, for example, potassium-promoted $NiMo/Al_2O_3$ [11] and Mo/Al_2O_3 [14] catalysts at 625–673 K. It also has been reported that the MoS_2/Al_2O_3 [15] and Ni–MoS/TiO_2 [12] catalysts exhibit high activity. Recently, transition metal carbides have been found to be useful in catalyzing this reaction. For the Mo carbides, Patt et al. reported high WGS activity with durability for the Mo carbide, which had an active site density >25% greater than that of the Cu–Zn catalyst [16]. Moon and Ryu also reported that the Mo carbide showed higher activity and stability for the WGS reaction than the commercial low-temperature CuZn catalyst [17]. Thus, molybdenum-containing carbides could have the bright prospect of developing into alternative catalysts for replacing the CuZn catalysts in the WGS reaction under the unstable oxidized operating conditions.

Despite these prospects, however, there have been a few reports about these catalysts' high performance in the WGS reaction at low temperature, the promoting effect of additive metals, the structures and surface properties of the molybdenum-containing carbides, and the relation to catalyst performance. In the present study, Co–Mo oxides with various compositions were carburized at various temperatures and tested for their

* Corresponding author.
E-mail address: mnagai@cc.tuat.ac.jp (M. Nagai).

0021-9517/$ – see front matter
doi:10.1016/j.jcat.2006.01.003

ability to catalyze the WGS reaction at the low temperature of 453 K. The relationship between the activities of these Co–Mo carbides for the WGS reaction and their structures and surface properties were studied by X-ray diffraction (XRD), N_2 and CO adsorption, transmission electron microscopy (TEM), temperature-programmed carburization (TPC), and X-ray photoelectron spectroscopy (XPS). The 873 K-carburized Co–Mo catalyst was also compared with the Co–Mo reduced at 873 K in 100% H_2 in terms of structure and catalytic activity. The mechanisms of the Co–Mo carbide formation were also investigated.

2. Experimental

2.1. Catalyst preparation

The oxidic precursors of the Co–Mo carbides with Co/(Co + Mo) ratios of 0, 0.10, 0.25, 0.35, 0.5, and 0.75 were prepared using a mixture of an aqueous solution of cobalt nitrate ($Co(NO_3)_2{\cdot}6H_2O$; Kishida Chemical Co., 99%) and an aqueous solution of ammonium heptamolybdate [$(NH_4)_6Mo_7O_{24}{\cdot}4H_2O$; Kishida Chemical Co., 99%]. The compounds were dissolved in water at 353 K with stirring, producing a viscous mixture. The solid products were placed in an oven, dried at 373 K overnight, heated at 773 K for 5 h, and then cooled to room temperature. The oxidized precursors (0.2 g) were placed on a porous quartz plate in a 10-nm-i.d. quartz microreactor, the ends of which were each connected to a 1/8-inch stainless steel tube. These were heated in dry air at a rate of 66.7 ml/min, oxidized at 723 K for 1 h, and then cooled to 573 K. The oxidized catalyst was purged at 573 K with He (15 ml/min) for 10 min, carburized by the temperature-programmed reaction in a stream of 20% CH_4/H_2 (66.7 ml/min) from 573 K to a final temperature of 823–1023 K at the rate of 1 K/min, and maintained at the final temperature for 2 h. The catalyst was cooled to 453 K in flowing 20% CH_4/H_2 and then purged with He for 10 min before the reaction. The carbide catalysts were removed from the microreactor and then transferred to a glove box, in which the atmosphere was exchanged five times with argon (99.9999%). The carbide catalysts were then used for characterization or the WGS reaction without exposure to air. The 873 K-reduced $Co_{0.5}Mo_{0.5}$ catalyst was prepared by the temperature-programmed reaction in a stream of 100% H_2 (66.7 ml/min) from 573 to 873 K at a rate of 1 K/min and maintained at 873 K in flowing H_2 for 2 h. A commercial CuZn catalyst (Süd-Chemie, AG) was also used in the reaction for comparison. Before the reaction, the temperature of the CuZn catalyst (0.2 g) was increased from room temperature to 473 K at a rate of 10 K/min in a stream of 10% H_2/He (15 ml/min), maintained at 473 K for 3 h, then lowered to 453 K in flowing He, after which the catalyst was purged with He (15 ml/min) for 10 min. The Co–Mo carbide catalysts are identified as $Co_xMo_{1-x}C\text{-}T_j$, where x and $1-x$ are the percentages of Co and Mo in the precursor compounds, respectively, and T_j is the carburizing temperature.

2.2. The WGS reaction

The WGS reaction was carried out at 453 K in a stream of 10.5% CO and 21% H_2O in a He balance gas at a flow rate of 60 ml/min. Water (ultra-pure) was pumped at a rate of 0.006 ml/min using a micropump (Lab-Quatec model LP-6300). CO, CO_2, and H_2 were quantitatively analyzed using an on-line gas chromatograph with a thermal conductivity detector (column, activated carbon; i.d., 6 mm; length, 2 m). The column temperature was initially held at 413 K for 6 min, after which it was increased from 413 to 473 K at a rate of 20 K/min, then held at 473 K for 6 min. The reaction gas was sampled at 30-min intervals, starting 5 min after the run and ending after 300 min.

2.3. Characterization

The BET surface areas of the catalysts were measured using an Omnisorp 100CX (Beckman Coulter) after the catalyst was evacuated at 473 K and 1.3×10^{-4} Pa for 2 h. The irreversible CO chemisorption was determined using an Omnisorp 100CX analyzer. Before the CO adsorption was measured, the catalysts were first heated from room temperature to 673 K at a rate of 10 K/min in a stream of He, purged at 673 K for 2 h, pretreated in a stream of H_2 at 623 K for 1 h, and then cooled to 303 K in a vacuum. For the pretreatment of CuZn, the catalyst was heated from room temperature to 423 K in a stream of He, purged in a stream of He for 2 h, and reduced at 423 K for 3 h in a stream of H_2. The bulk structures of the oxide and carbide materials were measured by XRD with a Rigaku RINT2000 using Cu-K_α radiation. The peaks were identified on the basis of the JCPDS card references for MoO_3, MoO_2, β-Mo_2C, CoO, Co_3O_4, Co metal, and $CoMoO_4$ (35-609, 32-671, 35-787, 43-1004, 43-1003, 15-806, and 21-868, respectively). Co_3Mo_3C was identified by comparing the following data: 80-0339, $2\theta = 39.9$, 42.4, and 46.4°. The mapping of the elements Co, Mo, C, and O and the surface structure of the $Co_{0.5}Mo_{0.5}C$-873 catalyst were analyzed using a JEM-2500SE transmission electron microscope (Japan Electronic Co.) with an energy dispersion analyzer (EDS). TPC of Mo and the $Co_{0.25}Mo_{0.75}$ oxides was studied to determine how the Co–Mo oxides were carburized during the carburization. TPC was carried out by heating from 573 to 973 K at a ramp rate of 10 K/min and maintaining the temperature at 973 K for 2 h, while monitoring the H_2O ($m/z = 18$) using a quadruple mass spectrometer (Quadstar 422, Balzer Co.). TPR was done in situ for the $Co_{0.5}Mo_{0.5}C$-873 catalysts by heating from 873 to 1220 K at a rate of 10 K/min in a 15-ml/min stream of H_2. XPS was performed with a Shimadzu ESCA 3200 photoelectron spectrometer using Mg-K_α. The experimental procedure involved removing the catalysts from the reactor after the carburizing treatment, transferring them to a glove box without exposure to air, mounting them on a holder with carbon tape while in the glove box, and then introducing them into the chamber. Argon etching was done for 1 min before measurement at a pressure of 5×10^{-6} Pa. The binding energies of Mo 3d and Co 2p were analyzed at 220–240 and 775–805 eV, respectively, using the

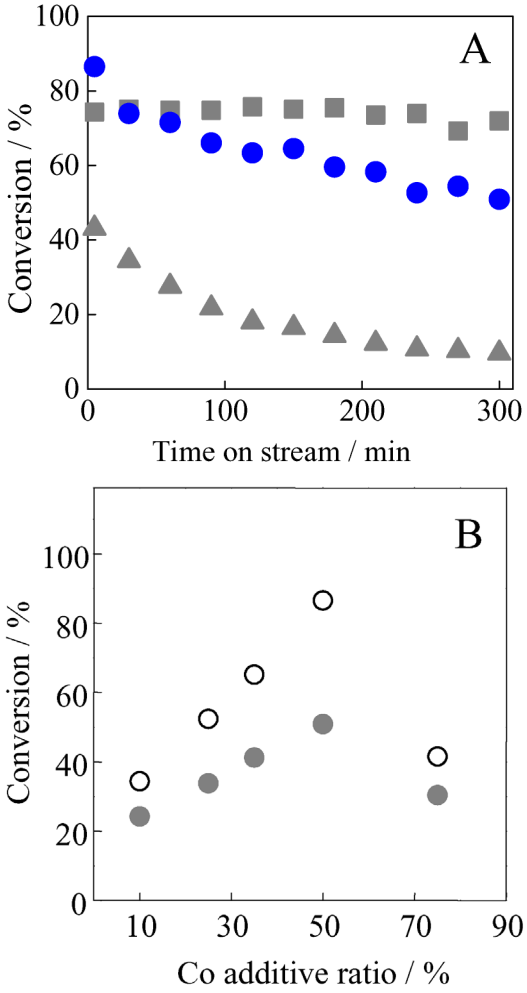

Fig. 1. (A) Conversion of CO to CO_2 over (●) $Co_{0.5}Mo_{0.5}C$-873, (▲) MoC-873, and (■) CuZn catalyst. (B) Conversion of CO to CO_2 at (○) 5 and (●) 300 min over the Co–Mo carbides with various Co/Mo ratios.

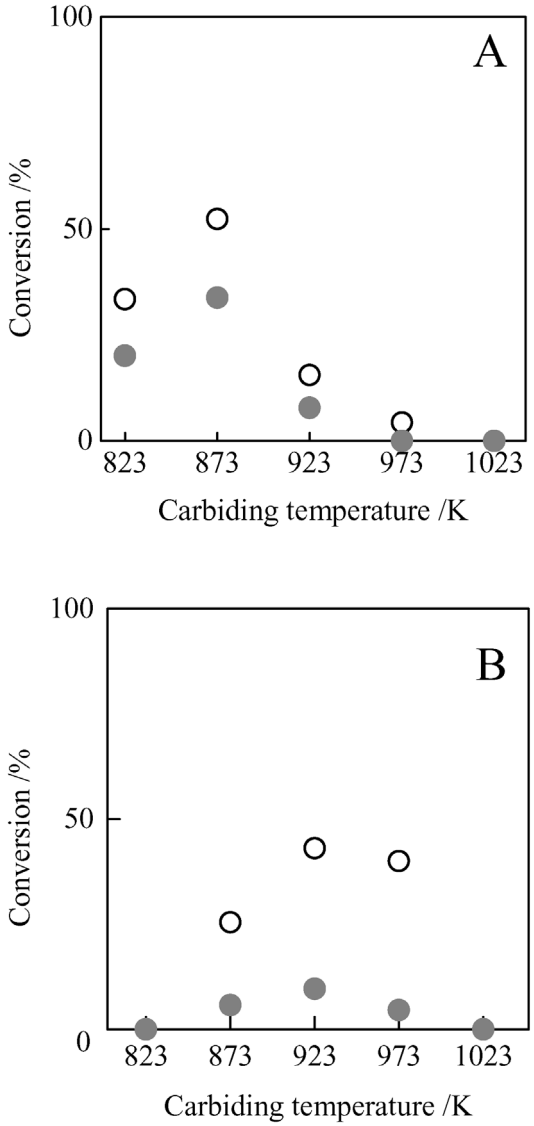

Fig. 2. Conversion of CO over (A) $Co_{0.25}Mo_{0.75}$ and (B) Mo catalysts carburized at various temperatures at (○) 5 and (●) 300 min.

Shirley baseline correction method. The binding energies of C 1s and O 2p were measured at 282.5–292.0 (for the carbidic and graphitic carbons) and 523–543 eV, respectively.

3. Results and discussion

3.1. The WGS reaction

The conversion of CO to CO_2 in the WGS reaction over MoC-923, $Co_{0.25}Mo_{0.75}C$-873, $Co_{0.5}Mo_{0.5}C$-873, and CuZn at 453 K is shown in Fig. 1A. The conversion rate at 5 min was higher for the $Co_{0.5}Mo_{0.5}C$-873 catalyst than for the commercial CuZn catalyst, although the activity of the Co–Mo catalyst gradually decreased, becoming less than that of the CuZn catalyst at 300 min. The MoC-923 was extremely less active than the $Co_{0.5}Mo_{0.5}C$-873 and CuZn catalysts. As shown in Fig. 1B, the CO conversion for the Co–Mo catalysts increased with increasing Co content up to 50%, and then decreased at a 75% cobalt content. The $Co_{0.5}Mo_{0.5}$ catalyst was the most active among the carbide catalysts with various Co contents. It is noteworthy that the $Co_{0.5}Mo_{0.5}C$-873 catalyst was more active than the commercial CuZn catalyst during the initial stage of the reaction. CO conversion for the WGS reaction over $Co_{0.25}Mo_{0.75}$ and Mo carburized at 823–973 K at the reaction temperature of 453 K is also shown in Fig. 2. The $Co_{0.25}Mo_{0.75}C$-873 was more active than the catalysts carburized at the other temperatures. Conversion by the $Co_{0.25}Mo_{0.75}C$-873 catalyst was higher than conversion by the MoC-923 catalyst.

These results suggest that the 25% Co content produced a 52% increase in conversion and a 50 K decrease in temperature for carburization of the Co–Mo oxides relative to that of Mo. Thus, the reactivity of the Co–Mo carbides catalysts with respect to the WGS reaction was very sensitive to the carburizing temperature, leading to the creation of various carbide species, such as each or both oxycarbides and carbides of cobalt and molybdenum. The CO chemisorption of the catalysts is characterized in Table 1. CO adsorption was 2.1 times higher in the $Co_{0.5}Mo_{0.5}C$-873 catalyst than in the CuZn catalyst. This result suggests that the Co–Mo carbide probably competed with CuZn in catalyzing the WGS reaction. $Co_{0.25}Mo_{0.75}C$-873 and

Table 1
BET surface areas, CO adsorption, and TOF for 873 K-carburized catalysts with various Co contents

Co content	BET surface area (m^2/g)	CO adsorption (μmol/g)	Reaction rate[b] (mmol/(min g))	TOF (min^{-1})
0[a]	26	18	0.306	17
10	76	58	0.287	5.0
25	67	45	0.431	9.6
35	74	65	0.544	8.4
50	94 ⟨88[c]⟩	70 ⟨64[c]⟩	0.719 ⟨0.419[c]⟩	10
75	49	35	0.345	9.9
CuZn	61 ⟨60[c]⟩	25	0.624	25

[a] 923 K-carburized Mo.
[b] At reaction time of 5 min.
[c] At reaction of 300 min.

MoC-923, with high CO adsorption, exhibited high catalytic activity (reaction rate and turnover frequency [TOF]) with respect to the WGS reaction. The TOF (rate of conversion of CO to CO_2 at 5 min over the irreversible CO uptake) of the CuZn catalyst was three times that of the Co–Mo carbides during the reaction. The TOF of the 873 K-carburized catalyst was greater than that of the catalysts at the other carburizing temperatures listed in Table 2.

3.2. The bulk structure and composition of Co–Mo carbide catalysts

The XRD patterns of the 873 K-carburized Co–Mo catalysts with various Co/(Co + Mo) ratios are shown in Fig. 3A. All of the carbide catalysts contained β-Mo_2C. The peak intensity of β-Mo_2C decreased with increasing Co content; especially above 35% Co content; all of the peaks became weaker, and the $Co_{0.5}Mo_{0.5}$ catalyst consisted of small peaks of β-Mo_2C and Co metal with a very weak Co_3Mo_3C peak. The sharp peaks of the Co metal with a small peak of Co_3Mo_3C were observed in $Co_{0.75}Mo_{0.25}$C-873. The XRD patterns of $Co_{0.25}Mo_{0.75}$ versus carburizing temperature are shown in Fig. 3B. Carburization of $Co_{0.25}Mo_{0.75}$ at 873–973 K produced mainly β-Mo_2C, whereas that at 823 K formed mainly MoO_2. The crystallinity of β-Mo_2C was low in the active $Co_{0.25}Mo_{0.75}$C-873 catalyst, but increased in the $Co_{0.25}Mo_{0.75}$C-973 catalyst. Newsam et al. [18] and Liang et al. [19] reported that the carburization of $Co_{0.5}Mo_{0.5}$ oxide with activated carbons in hydrogen at 873 K formed a η-type Co–Mo carbide structure, identical to that in the bimetallic carbide $Co_6Mo_6C_2$ [18,19] and Co_3Mo_3C [20]. Co_6Mo_6C [18] was formed when $Co(en)_3MoO_4$ was heated in a H_2/He flow and allowed to react with CO/CO_2 mixtures at 1273 K. In this study, the active $Co_{0.5}Mo_{0.5}$C-873 catalyst did not have a distinct structure but was amorphous, and $Co_{0.75}Mo_{0.25}$C-873 contained a small amount of Co_3Mo_3C. The formation of this amorphous carbide led to a high surface area and high catalytic activity with respect to the WGS reaction. In addition, the patterns of the peaks for the catalysts after the reaction were the same as those before the reaction, and no crystals grew for 300 min during the reaction.

The BET surface areas of Mo and the Co–Mo carbides are shown in Tables 1 and 2. The carburization of the Co–Mo oxides markedly increased the surface area of $Co_{0.1}Mo_{0.9}$-873, to 76 m^2/g, from the 3 m^2/g of MoC-823/873. The $Co_{0.5}Mo_{0.5}$ catalyst exhibited the highest surface area (94 m^2/g) of all the bulk carbide catalysts. Korlann et al. [20] reported a BET surface area of 111 m^2/g for the 20 wt% Co_3Mo_3C/Al_2O_3 through the topotactic preparation of the Co–Mo carbide by the temperature-programmed reaction of Co_3Mo_3N from 673 to 950 K in 20% CH_4/H_2. The incomplete carburizing preparation of the unsupported Co–Mo carbide from 573 to 873 K for 3 h in this study can provide a high-surface area Co–Mo carbide.

STEM images and element mappings for the total image, molybdenum, cobalt, and carbon for the STEM analysis of the $Co_{0.5}Mo_{0.5}$C-873 catalyst are shown in Fig. 4A. The element image of the Mo atom overlapped that of the C atom at the dark portion of the STEM image, indicating that almost all of the molybdenum and carbon were equally distributed to form the Mo carbide. For Co, the darker portion corresponded to that of the total element mapping, showing that the presence of Co was locally distributed on the surface of Mo_2C. TEM images of the surface structure of the $Co_{0.5}Mo_{0.5}$C-873 catalyst is shown in Figs. 4B and C. The structure is a hexagonal closed packing of the β-Mo_2C (0001)-phase lattice, but the lattices are scattered in parts of the Mo-rich region; see Fig. 4B (a). The amorphous substance is seen in the spotted stripes on the β-Mo_2C surface. All of the crystals consisted mainly of β-Mo_2C with amorphous cobalt species, such as the amorphous Co–Mo carbide. In the Co-rich region [Fig. 4C (c)], not all lattices could be observed, and the crystals were likely amorphous. On the total surface, the spotted-stripe patterns could not be clearly observed, and but they likely dominated the surface area structure of the catalysts.

The XRD pattern of $Co_{0.5}Mo_{0.5}$ reduced at 873 K in a stream of H_2 is shown in Fig. 5, and it clarifies the difference between treating the Co–Mo oxide at 873 K in a stream of H_2 and treating it in 20% CH_4/H_2. The reduced $Co_{0.5}Mo_{0.5}$ catalyst exhibited the XRD peaks of Co_3Mo and Mo metal at low intensities without Co_3Mo_3C and Co metal and with the surface area of 55 m^2/g. The reduced Co–Mo catalyst exhibited no catalytic

Table 2
BET surface area, CO adsorption, and TOF for Mo and $Co_{0.25}Mo_{0.75}$ carburized at various temperatures

	BET surface area (m^2/g)		CO adsorption (μmol/g)		Reaction rate (mmol/(min g))		TOF (min^{-1})	
	Mo	$Co_{0.25}Mo_{0.75}$	Mo	$Co_{0.25}Mo_{0.75}$	Mo	$Co_{0.25}Mo_{0.75}$	Mo	$Co_{0.25}Mo_{0.75}$
823	3	15	5	44	0.005	0.273	1	6.2
873	3	67	8	45	0.193	0.431	24	9.6
923	26	12	18	19	0.306	0.100	17	5.3
973	7	11	5	18	0.279	0.009	56	0.5

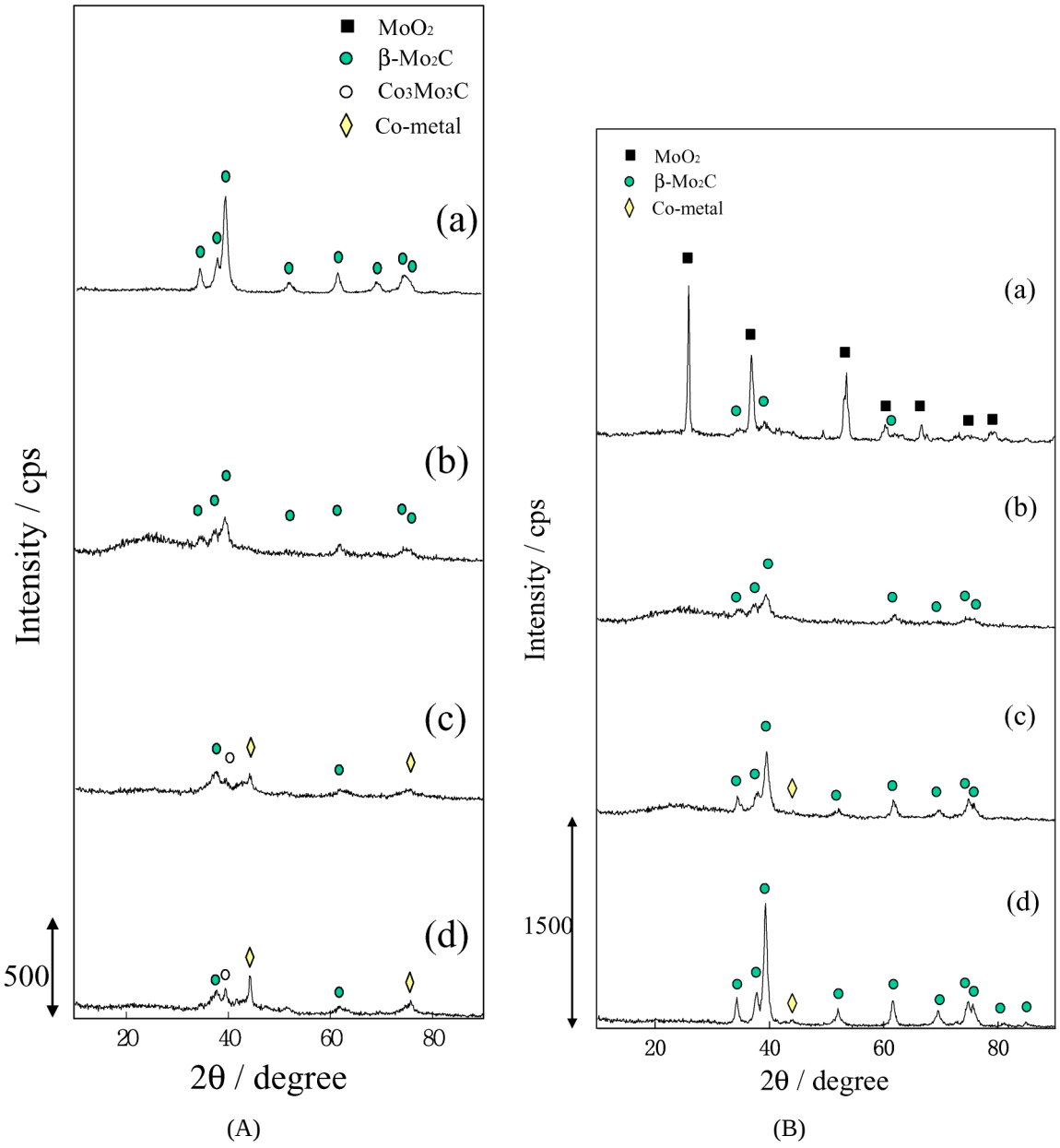

Fig. 3. XRD patterns of (A): (a) MoC-873, (b) $Co_{0.25}Mo_{0.75}C$-873, (c) $Co_{0.5}Mo_{0.5}C$-873, and (d) $Co_{0.75}Mo_{0.25}C$-873, and (B): $Co_{0.25}Mo_{0.75}$ catalysts carburized at (a) 823, (b) 873, (c) 923, and (d) 973 K.

activity for the WGS reaction. In contrast, the $Co_{0.5}Mo_{0.5}C$-873 catalyst in the 20% CH_4/H_2 mixture consisted of fine particles with a high surface area (94 m^2/g). As a result, the reduced catalyst did not contain the active Co–Mo carbides, which differed in structure from the carbide catalyst.

3.3. Carburization of the Co–Mo oxide

The profile of the H_2O ($m/z = 18$) desorption during the TPC of MoO_3 and $Co_{0.25}Mo_{0.75}$, based on the suitable carburization temperature that can be determined, is shown in Fig. 6. The desorption of H_2O was observed for Mo and $Co_{0.25}Mo_{0.75}$ at two peaks of low temperature (780 and 747 K, respectively) and high temperature (945 and 893 K, respectively), during the TPC. The high-temperature peak for $Co_{0.25}Mo_{0.75}$ shifted by 52 K to a temperature lower than that for Mo. The carburizing temperatures at 873 K for the $Co_{0.25}Mo_{0.75}$ oxide and at 923 K for the Mo oxide were 20–22 K lower than the two high-temperature peaks of H_2O in the TPC. This result shows that the bimetallic Co–Mo oxides were not completely carburized at 873 K and that oxygen remained in some parts, which then generated the amorphous Co–Mo oxycarbides. This result agrees with the high WGS activity data. Combining the TPC and XRD results, it is clear that the first desorption peak of H_2O at 747 K was due to the reduction and/or carburization of MoO_3 to MoO_2 and Mo oxycarbide (MoC_yO_z) and of $CoMoO_4$ to Co–Mo oxycarbide ($CoMoC_yO_z$),

$$MoO_3 \xrightarrow{20\%CH_4/H_2} MoO_2 + MoC_yO_z$$

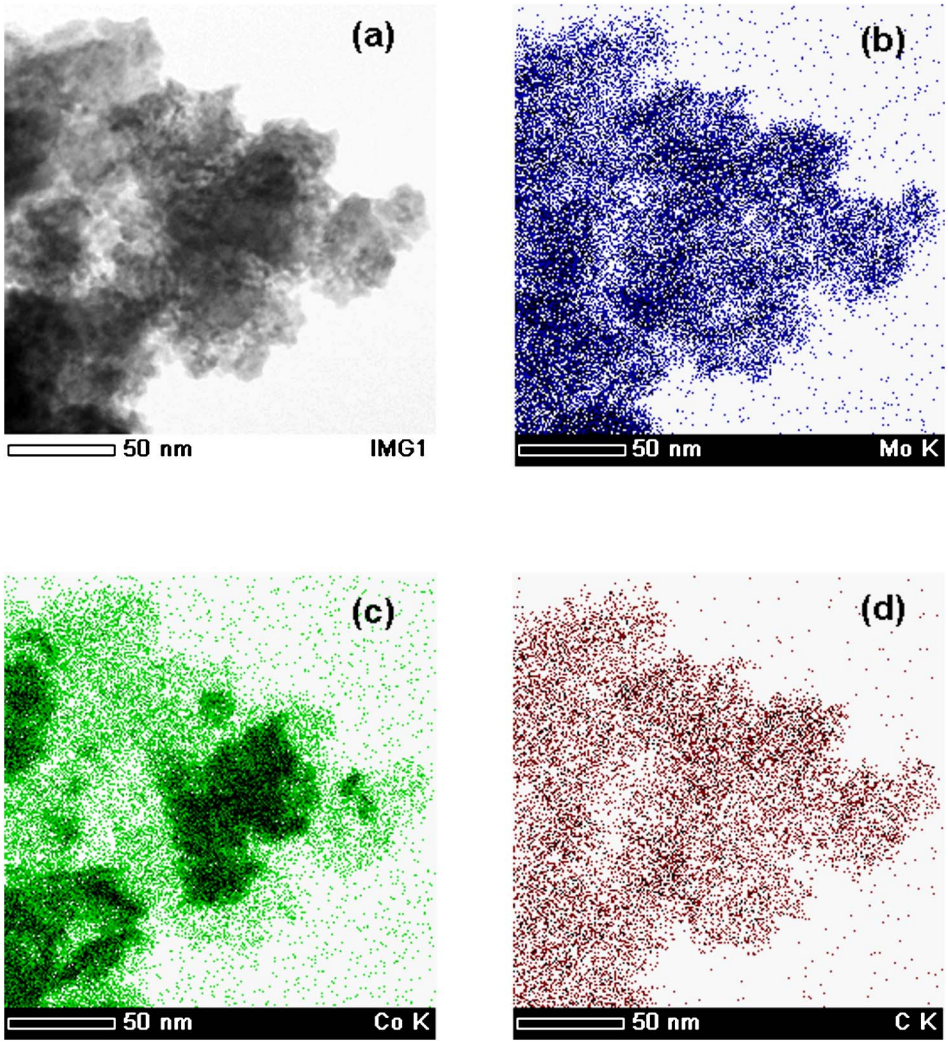

(A)

Fig. 4. (A) Element of $Co_{0.5}Mo_{0.5}C$-873. (a) STEM imaging and mapping of (b) molybdenum, (c) cobalt, and (d) carbon. High resolution TEM photographs of $Co_{0.5}Mo_{0.5}C$-873 in (B) molybdenum-rich and (C) cobalt-rich regions. Regarding (B), (b) is the color reversal of (a). Regarding (C), (d) is the color reversals of (c).

and

$$CoMoO_4 \xrightarrow{20\%CH_4/H_2} CoMoC_yO_z.$$

The desorption peak of H_2O in the saddle region at 747–893 K is due to the start of the carburization of $MoO_2 + MoC_yO_z$ to β-Mo_2C and of $CoMoC_yO_z$ to Co–Mo carbide ($CoMoC_y$), as well as the completion of the first process of the reduction and/or carburization. The desorption peak at 893 K was due to the carburization of MoC_yO_z to β-Mo_2C and subsequently the amorphous $CoMoC_y$ with Co metal,

$$MoC_yO_z \xrightarrow{20\%CH_4/H_2} \beta\text{-}Mo_2C$$

and

$$CoMoC_yO_z \xrightarrow{20\%CH_4/H_2} CoMoC_y + \text{Co metal}.$$

Xiao et al. [21] reported the presence of a high-temperature peak smaller than the low-temperature peak found during the TPC preparation of $Co_{0.5}Mo_{0.5}$ oxide in a stream of the 10% C_2H_6/H_2 mixture. The carburizing treatment in a stream of 20% CH_4/H_2 readily formed the Co–Mo oxycarbide from $CoMoO_4$. Furthermore, the C/(Co + Mo) ratio for the Co–Mo carbides for the 35 and 50% Co contents was higher than that at the 25% Co loading, as can be seen in Table 3. The most active $Co_{0.5}Mo_{0.5}$ oxycarbide had the composition $CoMoC_{6.2}O_{1.4}$, which contains a large amount of carbons and less oxygen than the other Co–Mo oxycarbides, such as $Co_{0.25}Mo_{0.75}C$-873. The promotion of WGS activity by the addition of cobalt at lower carburizing temperatures is probably due to either the activation of hydrogen atoms by Co metal [19] or the Co spillover hydrogen from H_2O to the Mo atoms on the contact layers of Co. To determine the amorphous structure of $Co_{0.5}Mo_{0.5}C$-873 by XRD, the sample was heated from 873 to 1223 K in a stream of H_2 after the TPC. The peaks of Co_3Mo_3C were observed in Fig. 7. It is reasonable to assume that the amorphous Co–Mo carbide was converted to the Co_3Mo_3C crystallite. Consequently, the active $Co_{0.5}Mo_{0.5}C$-873 contained only amorphous Co_3Mo_3C. The formation of this amorphous Co–Mo carbide led to a high surface area and high catalytic activity with respect to the WGS reaction.

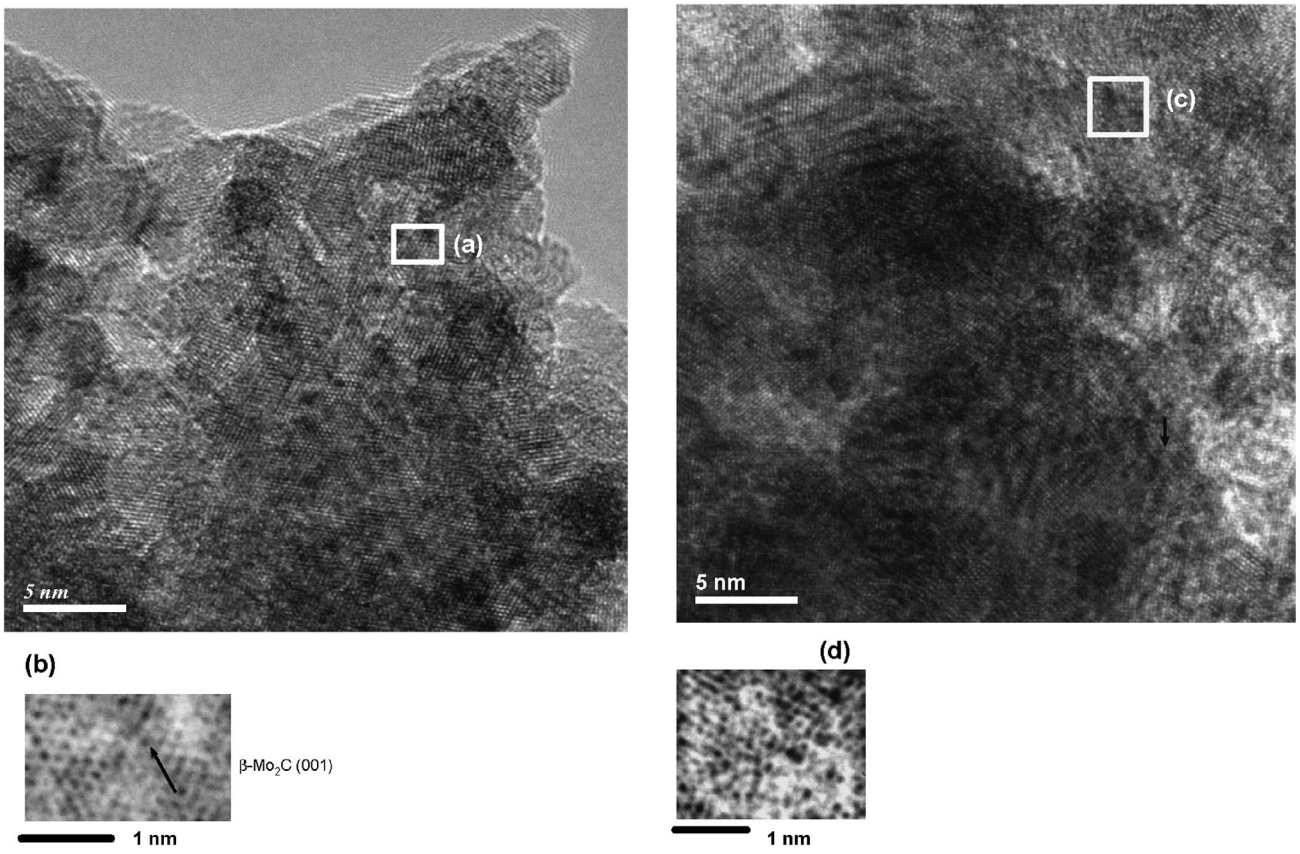

Fig. 4. (*continued*).

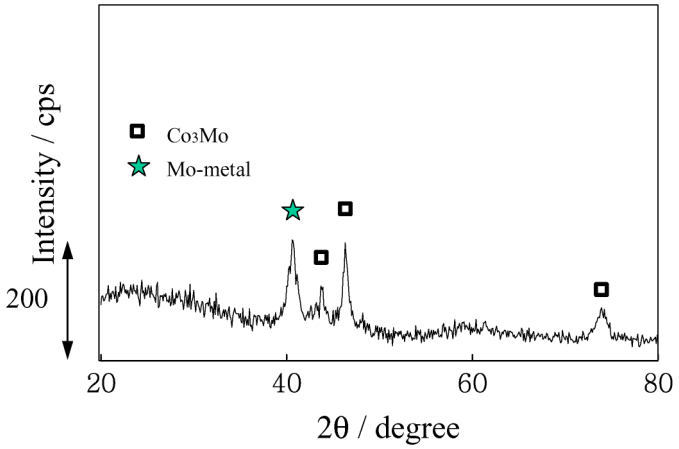

Fig. 5. XRD patterns of $Co_{0.5}Mo_{0.5}$ reduced at 873 K in a stream of hydrogen.

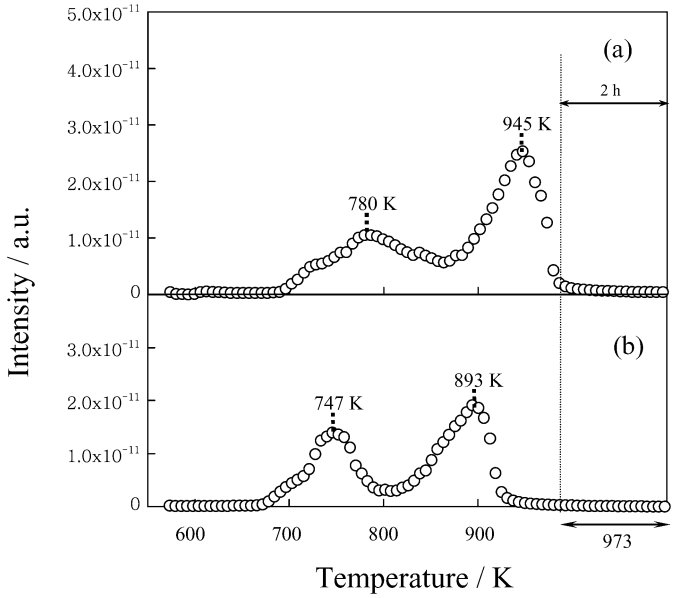

Fig. 6. Desorption of H_2O during temperature-programmed carburization of (a) Mo oxide and (b) $Co_{0.25}Mo_{0.75}$ oxide from room temperature to 973 K at the damp rate of 1 K/min and kept at 973 K for 2 h.

3.4. Active species

The $Co_{0.5}Mo_{0.5}C$-873 catalyst exhibited a high activity for the WGS reaction and contained small $CoMoC_yO_z$ particles. This increase in activity is likely due to the increase in the carbon-deficient sites and the Co atoms of the Co–Mo carbides. The increase in the Co produced fine particles of the Co–Mo oxycarbide from β-Mo_2C and caused a high CO adsorption. In a previous paper, β-$Mo_2C_{0.8}$ with many carbon-deficient sites was reported to exhibit a much higher CO adsorption than the complete crystallite of β-Mo_2C, according to a Monte Carlo simulation [22]. The Co–Mo oxycarbide had many carbon-deficient sites of Co_3Mo_3C crystallites. On what catalyst sites were the CO and H_2O adsorbed during the WGS reaction?

Table 3
Atomic ratios of C/(Co + Mo) and O/(Co + Mo) for $Co_{0.25}Mo_{0.75}C$-873 catalysts

Co content	Atomic ratio	
	C/(Co + Mo)	O/(Co + Mo)
0	5.3	2.4
10	2.5	1.7
25	2.1	1.4
35	3.0	0.9
50	3.1	0.7

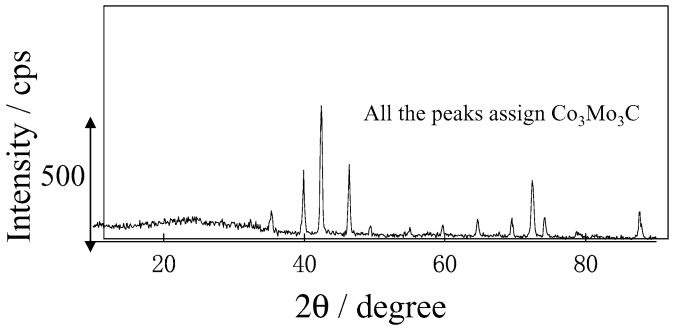

Fig. 7. XRD patterns of $Co_{0.5}Mo_{0.5}C$-873 heated from 873 to 1123 K in a stream of hydrogen after TPC.

In terms of the CO adsorption, CO preferentially adsorbed on the carbon-deficient sites of α-$Mo_2C(0001)$ and diffused into the domain, according to the former CO-adsorption STM results [23]. Clair et al. [24] proposed that ca. 85% of the surface oxygen from split CO did not burn off as CO, but instead diffused into the α-$Mo_2C(0001)$ bulk. This suggests that CO molecularly adsorbs on the Co- and C-terminated surface defect sites of the CoMo carbides, rather than dissociating on the surface. As for water, Hwu et al. [25] reported that H_2O molecules dissociated into hydrogen and surface hydroxyl groups, which decomposed into hydrogen and surface oxygen on C/W(111) at 330 K. They also suggested that the hydroxyl may well migrate to the electron-rich carbon; the surface carbon participated on the carbide, leading to the conversion of CO to CO_2. Very recently, Tominaga and Nagai [26] studied the DFT of the WGS reaction over β-$Mo_2C(001)$ and reported that β-Mo_2C dissociated H_2O into H and O atoms and that CO approached the O atom to form CO_2. In this study, water reacted with the adsorbed CO or carbidic carbons of the catalyst to produce H_2 and CO_2. It is postulated that the promoting effect of the Co atom is the diffusion of the spillover hydrogen from H_2O to the Mo atoms on the contact layers of the cobalt.

4. Conclusion

Active Co–Mo carbides catalyzing the WGS reaction were studied on the basis of CO, XRD, TEM, and XPS. $Co_{0.5}Mo_{0.5}C$-873 was found to be the most active among the catalysts studied. This carbide catalyst was more active than CuZn at 5 min but less active than CuZn at 300 min into the reaction. CO adsorption of $Co_{0.5}Mo_{0.5}C$-873 exceeded that on the CuZn catalyst. Based on the TPC analysis, the $Co_{0.25}Mo_{0.75}C$-873 exhibited H_2O desorption peaks at 747 and 893 K, with the former peak ascribed to the formation of Co–Mo oxycarbide from the oxide and the latter peak ascribed to the formation of Co–Mo carbide from the oxycarbide. The $Co_{0.5}Mo_{0.5}C$-873 contained Co–Mo oxycarbide with β-Mo_2C and Co metal and probably consisted of β-Mo_2C with amorphous cobalt species. The incomplete carburization of the Co–Mo oxide formed the amorphous Co–Mo oxycarbide, leading to a high activity for the WGS reaction. Water reacted with the adsorbed CO or carbidic carbons to the produce hydrogen and carbon dioxide in the gas phase.

Acknowledgments

This work was carried out as a research project using a Grant-In-Aid for Scientific Research from the Japanese Ministry of Education, Sport, Culture, and Science.

References

[1] C. Rhodes, G.J. Hutchings, A.M. Ward, Catal. Today 23 (1995) 43.
[2] T. Utaka, K. Sekizawa, K. Eguchi, Appl. Catal. A 194–195 (2000) 21.
[3] Y. Tanaka, T. Utaka, R. Kikuchi, T. Takeguchi, K. Sasaki, K. Eguchi, J. Catal. 215 (2003) 271.
[4] N.A. Koryabkina, A.A. Phatak, W.F. Ruettinger, R.J. Farrauto, F.H. Ribeiro, J. Catal. 217 (2003) 233.
[5] S. Zhao, T. Luo, R.J. Gorte, J. Catal. 221 (2004) 413.
[6] P. Ratnasamy, D. Srinivas, C.V.V. Satyanarayana, P. Manikandan, R.S.S. Kumaran, M. Sachin, V.N. Shetti, J. Catal. 221 (2004) 455.
[7] Y. Hu, H. Jin, J. Liu, D. Hao, Chem. Eng. J. 78 (2000) 147.
[8] Y. Li, Q. Fu, M. Flytzani-Stephanopoulos, Appl. Catal. B 27 (2000) 179.
[9] I. Balint, K. Aika, Appl. Catal. A 196 (2000) 209.
[10] Y. Tanaka, T. Utaka, R. Kikuchi, T. Takeguchi, K. Sasaki, K. Eguchi, J. Catal. 215 (2003) 271.
[11] M. Kantschewa, F. Delannay, H. Jeziorowski, E. Delgado, S. Eder, G. Ertl, H. Knözinger, J. Catal. 87 (1984) 482.
[12] M. Laniecki, M. Malecka-Grycz, F. Domka, Appl. Catal. A 196 (2000) 293.
[13] M.A. Segura, C.L. Aldridge, K.L. Riley, US Patent (1977) 4054644.
[14] R.N. Nickolov, R.M. Edreva-Kardjieva, V.J. Kafedjiysky, D.A. Nikolova, N.B. Stankova, D.R. Mehandjiev, Appl. Catal. A 190 (2000) 191.
[15] P. Hou, D. Meeker, H. Wise, J. Catal. 80 (1983) 280.
[16] J. Patt, D.J. Moon, C. Phillips, L. Thompson, Catal. Lett. 65 (2000) 193.
[17] D.J. Moon, J.W. Ryu, Catal. Lett. 92 (2004) 17.
[18] J.M. Newsam, A.J. Jacobson, L.E. McCandlish, R.S. Polizzotti, J. Solid State Chem. 75 (1988) 296.
[19] C. Liang, W. Ma, Z. Feng, C. Li, Carbon 41 (2003) 1833.
[20] S. Korlann, B. Diaz, M.E. Bussell, Chem. Mater. 14 (2002) 4049.
[21] T.-C. Xiao, A.P.E. York, H. Al-Megren, C.V. Williams, H.-T. Wang, M.L.H. Green, J. Catal. 202 (2001) 100.
[22] M. Nagai, H. Tominaga, S. Omi, Langnuir 16 (2000) 10215.
[23] R.-L. Lo, K. Fukui, S. Otani, S.T. Oyama, Y. Iwasawa, Jpn. J. Appl. Phys. 38 (1999) 3813.
[24] T.P.St. Clair, S.T. Oyama, D.F. Cox, Surf. Sci. 468 (2000) 62.
[25] H.H. Hwu, B.D. Polizzotti, J.G. Chen, J. Phys. Chem. B 105 (2001) 10045.
[26] H. Tominaga, M. Nagai, J. Phys. Chem. B 109 (2005) 20415.